applied sciences

MDPI

*Article*

# Effects of Grout Compactness on the Tensile Behavior of Grouted Splice Sleeve Connectors

**Zhangrong Zhang [1], Shaofei Jiang [1,2,*], Wanxia Cai [1] and Chunming Zhang [3]**

[1] Department of Civil Engineering, Fuzhou University, Fuzhou 350116, China; cezrzhang@163.com (Z.Z.); wxCai202204@163.com (W.C.)
[2] Fujian Provincial Key Laboratory on Multi-Disasters Prevention and Mitigation in Civil Engineering, Fuzhou 350108, China
[3] Department of Resources and Civil Engineering, Northeastern University, Shenyang 110004, China; mrzhang2001@163.com
* Correspondence: cejsf@fzu.edu.cn; Tel.: +86-591-2286-5379

**Abstract:** The quality of grouted sleeve has a significant influence on the performance of the sleeve splice. Incompactness of the infilled grout is inevitable in sleeve grouting. To investigate the tensile behavior of grouted splice sleeves due to different grout compactness, monotonic tensile tests on grouted splice sleeve connectors were performed at grout compactness of 100%, 90%, 70%, and 50%, respectively. The bond-slip analytical model of rebar-grout was deduced by fitting the tensile test data, and the formula for the tensile capacity of the grouted splice sleeve was proposed in the paper. The results show that the tensile strength of the splice sleeve reduces as the grout compactness decreases. It was found from the experiment that the calculated values of tensile capacity are in good agreement with the experimental values. The proposed formula can be adopted in determining whether reinforcing remedies or re-grouting should be taken in the case of incompact grout in grouted splice sleeve connectors.

**Keywords:** grout compactness; precast concrete; grouted splice sleeve connector; tensile capacity; bond-slip analytical model



**Citation:** Zhang, Z.; Jiang, S.; Cai, W.; Zhang, C. Effects of Grout Compactness on the Tensile Behavior of Grouted Splice Sleeve Connectors. *Appl. Sci.* **2022**, *12*, 4595. https://doi.org/10.3390/app12094595

Academic Editor: Andrea Paglietti

Received: 1 April 2022
Accepted: 28 April 2022
Published: 1 May 2022



## 1. Introduction

Precast concrete construction is one of the main structural forms that has been widely adopted in China's construction industry. Compared with cast-in-place construction, the integrity and connection quality of precast concrete construction are critical for the safety and performance of the structure. Among all connection methods, the wet connection using grouted splice sleeve (GSS) is widely employed, which uses non-shrinkage grouting materials as bonding materials to ensure the continuity of load transfer. Sleeves are usually made by casting or machinery processing [1]. Grouting material uses cement as base material. After adding water and mixing with fine aggregate and a dry mix made of concrete admixture and other materials, the grouting material will have good fluidity, early strength, high strength, and minimum inflation [2].

The grout quality of GSS is, in a sense, covered in a black box. The factors affecting the grout quality of beam-reinforcement connecting sleeves are elusive and not always under control. For example, workers may not strictly abide by relevant construction standards, or in another case, grout slurry bleeding occurs during construction. Sleeves may have poor compactness and disengaging ends. These can result in bending failure, and excessive tensile stress at the connectors, presenting a safety risk to the operation of the fabricated buildings. The grout compactness has a certain impact on the mechanical properties of grouted splice sleeve connectors. However, no related research has been reported. To date, most studies focus on the monotonic tensile behavior of grouted splice sleeves in various forms due to factors such as production process, external shapes, and cavity structure [3].

Recently, only fully compact connectors are considered in the calculation of the tensile capacity of grouted splice sleeves. For example, Ling et al. [4] studied two types of grouted sleeves, namely the welded bar sleeve (WBS) and the tapered head sleeve (THS). By fitting the tensile test data of 18 fully compact sleeve connectors (9 WBS and 9 THS), they established a bond-slip model describing the tensile behavior of the reinforcement grout. The predicted tensile capacity of the sleeve connectors was obtained by referring to the tensile capacity of the connector reinforcement. The results showed that the predicted values of the tensile capacity of sleeve connector are within 10% deviation from the experimental results. During the past decade in China, research on grouted splice sleeve technology was mainly concentrated on studying the tensile behaviors of sleeve connectors in view of various factors, such as grout age and rebar types [5], outer shape, and inner cavity structure [6–9]. With the fast development of precast concrete structure manufacturing and construction technology, the shear-resistant and seismic-resistant performance of GSS has attracted increasing attention in recent years [10–15]. For instance, Tullini and Minghini [10] studied three monotonic tests (axial tension and four-point bending with and without axial compression) and two cyclic tests (four-point bending and shear) on precast reinforced concrete column-to-column connections with GSSs. Xu et al. [11] developed a full-scale precast reinforced concrete shear wall (PRCSW) endowed with single-row grout-filled sleeves connection, and conducted seismic experiments and numerical simulation of six-story precast box-modularized structures. Furthermore, the PRCSW specimen resembled the cast-in-place shear wall to study the performance design indices, such as failure modes, inter-story drift angle, ultimate force, ductility, and dissipated hysteretic energy. Popa et al. [12] conducted experiments on precast columns connected by grouted corrugated steel sleeves, and a comparison with reference cast-in-place specimens was made. The results show that the precast specimens have similar hysteretic response and energy dissipation capacity as the reference ones. Ameli et al. [13] presented a simplified modeling strategy for seismic assessment of precast bridge columns that were connected to precast footings using GSS connectors. A computational model was developed and validated using three half-scale bridge subassemblies. The results from the proposed computational model were found to be in good agreement with the experimental results.

The grout compactness has a great effect on the mechanical properties of the grouted splice sleeve, and thereby, the precast concrete buildings. Scholars have paid attention to developing the monitoring and detection methods for grout compactness and GSS [16–21]. Jiang et al. [16] presented a stress wave-based active sensing approach using piezoceramic transducers to monitor the grouting compactness in real-time. Liu et al. [17] employed the impact-echo method to study the grouting compactness of the grout sleeve. While other scholars paid attention to the mechanical properties of the GSS, Huang et al. [18] studied the tensile behavior of 15 half-grouted sleeve connections, and thus, an analytical model was proposed to predict the ultimate tensile capacity of the connections. To improve the performance of GSS, Zheng et al. [19] developed a new type of grout-filled coupling sleeve, and 11 coupler specimens of four categories with embedment lengths from 7 to 7.5 times bar diameter were prepared and tested under tensile load to study the mechanical performance. Parks et al. used the acoustic emission method to investigate the monotonic tensile behavior and quasi-static cyclic behavior of GSS connectors and the performance of reinforced precast concrete bridge assemblies connected by GSS [20,21]. Twenty-four specimens were conducted by Chen [22] to study the effects of spliced rebars with different diameters on the mechanics of GSS. The mechanical properties of different structural components, such as column, beam, and shear walls connected by GSS, were also studied in recent years, and the results showed that GSS could be an effective solution for the promotion of precast structures [23–25].

Overall, although both the detection methods of grout compactness and the study on mechanical properties of new GSS can greatly improve the performance of GSS and are beneficial to the application of grouted splice sleeves in practical engineering, there is no direct linking between them. Furthermore, the effect of the grout compactness on the

tensile bearing capacity of GSS connectors has not been reported. The grout compactness has a great effect on the mechanical properties of the grouted splice sleeve. The authors also propose a method to calculate the tensile bearing capacity of the grouted splice sleeve with the grout compactness into consideration. The method can be used to determine whether reinforcing remedies or re-grout is required in the case of incompact sleeve grouting during construction. Experiments were conducted on four types of GSS that were subjected to monotonic tensile loads. They have compactness of 100%, 90%, 70%, and 50%, respectively. The bond-slip model describing the relation of rebar-grout was, thus, deduced by fitting the monotonic tensile test data, and the tensile capacity calculation method of GSS is further studied.

The objective of this paper is two-fold: (1) to study the effect of grout compactness on the performance of GSS and (2) to propose an assessment method for the tensile bearing capacity of GSS in case of incompact grouting. The rest of the paper is organized as follows: Section 2 introduces the monotonic tensile tests of GSS with different compactness. An analytical method for the tensile bearing capacity of GSS is presented in Section 3. Section 4 draws the conclusions.

## 2. Tensile Tests on GSS Connectors with Different Compactness

In the experiments, four types of GSS with 100%, 90%, 70%, and 50% grout compactness, were subjected to monotonic tensile loads to study their failure modes, tensile capacity, stress, and strain distribution along the rebar and the sleeve. It is recognized that with the material and grout quality guaranteed, the angle between the two opposite reinforcement ribs and their misalignment are the reasons for sleeve connection failure. As for the sleeve studied in this paper, one end is equipped with ribs in the inner wall to hook the reinforcement, and the other end with an annular rubber plug to fix another reinforcement for positioning and alignment.

### 2.1. Preparation of GSS

The sleeves used in the experiments were manufactured by Shanghai Jusong Engineering Material Corporation, and they were cast from ductile iron. Four types of rebar with a nominal diameter $d$ of 18 mm, 20 mm, 22 mm, and 25 mm were used, denoted as D18, D20, D22, and D25, respectively. The length of rebars and sleeves were designed according to the core [26], as shown in Figure 1. More specifically, $L$ is the length of the sleeves, $L_1$ is the gauge length of elongation, $D_g$ is the outer diameter of the sleeves, $d_{si}$ is the inter diameter of the sleeves, and $t_{sl}$ is the pipe thickness of the sleeves. Their dimensions are shown in Table 1. The strength grade of the special purpose grouting material was $M80$. Manual pressure grouting was adopted for sleeve grouting, and the grouting tool was shown in Figure 2. The expansion agent was added in the grouting material in order to fill pores in the hardening process. Therefore, it is feasible to classify the compactness of grouted sleeves by controlling the volume of grouting material. Figures 3 and 4 show the schematic diagram and pictures of four compactness cases (100%, 90%, 70%, and 50% compactness), respectively. After grouting, the connectors were cured at a temperature of 20 °C and relative humidity of 90% for 28 days. After curing, the specimens were placed in a normal indoor environment for tensile loading tests [2]. For each type of GSS (D18, D20, D22, D25), three specimens were fabricated in accordance with the technical specification [26].

**Table 1.** The dimensions of the sleeves.

| Types of Sleeves | Length $L$/mm | Outer Diameter $D$/mm | Pipe Thickness $t_{sl}$/mm | Inner Diameter $d_{si}$/mm |
|---|---|---|---|---|
| D18 | 348.0 | 48.0 | 4.0 | 40.0 |
| D20 | 380.0 | 51.0 | 4.5 | 42.0 |
| D22 | 412.0 | 54.4 | 5.2 | 44.0 |
| D25 | 460.0 | 59.4 | 6.2 | 47.0 |

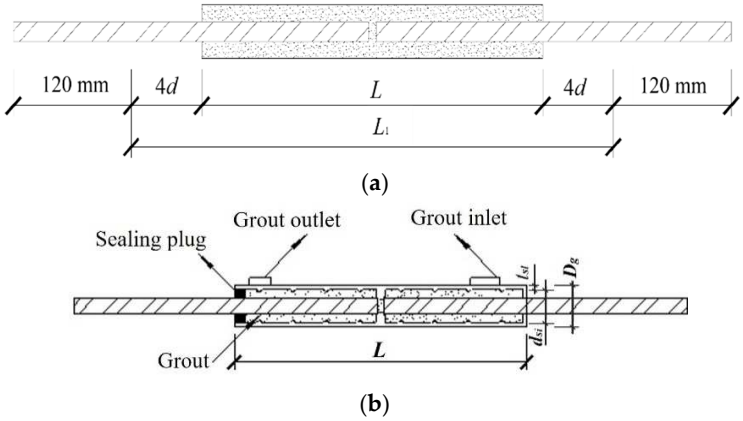


**Figure 1.** Schematic diagrams of grout sleeve. (**a**) Dimensions of grout sleeve and rebar. (**b**) Details of grout sleeve.

**Figure 2.** Schematic diagrams of grout sleeve.

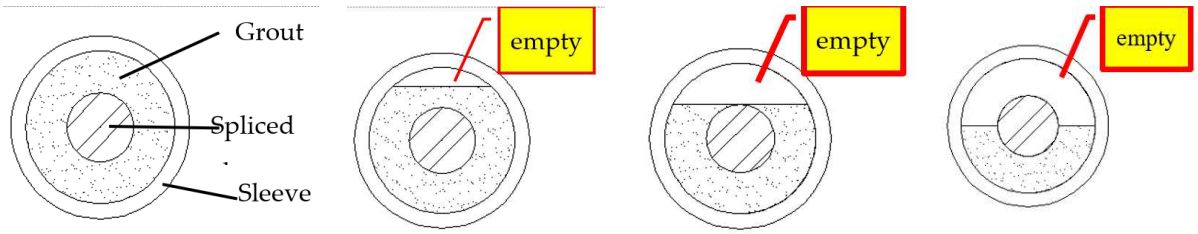


**Figure 3.** Schematic diagrams of different grout compactness. (**a**) 100% compactness. (**b**) 90% compactness. (**c**) 70% compactness. (**d**) 50% compactness.

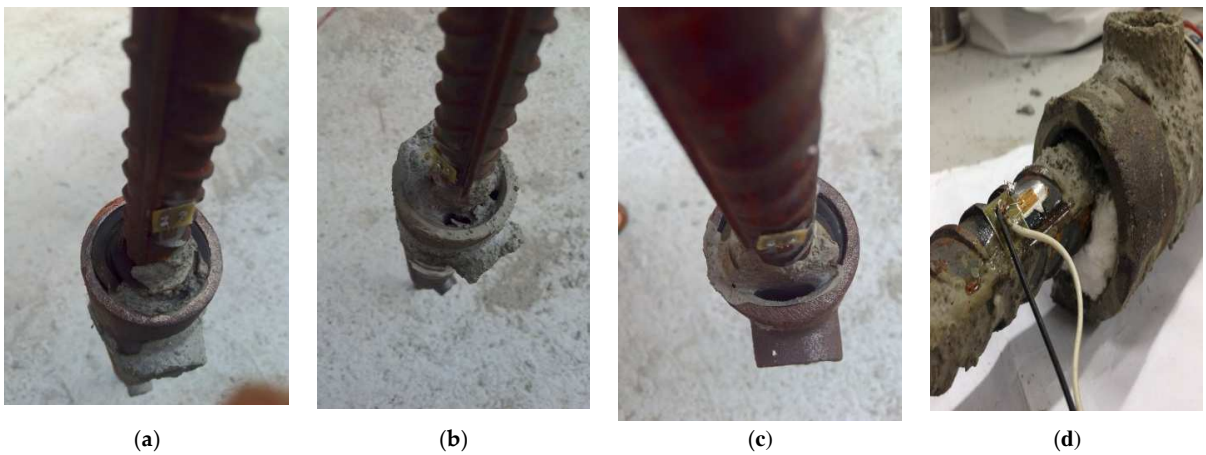


**Figure 4.** Pictures of different grout compactness. (**a**) 100% compactness. (**b**) 90% compactness. (**c**) 70% compactness. (**d**) 50% compactness.

### 2.2. Test Setup and Loading Process

To determine the material property, nine 40 mm × 40 mm × 160 mm prismatic specimens in three groups were fabricated. They were cured under the same condition as the GSS in line with Grouting Material for Steel Sleeve Connection [2] and Strength Testing Method for Cement Mortar [27]. After curing, the average compressive strength of the grout was measured at a loading rate of 2400 ± 200 N/s, and the compressive strength is 88.5 MPa, and more details were shown in Table 2. The strength grade of the spliced rebar is HRB400 [28]. The material properties of the four types of rebar, with three specimens each, were obtained in accordance with Tensile Testing of Metallic Materials-Part 1: Test Methods at Room Temperature [29], and the average mechanical properties are shown in Table 3.

**Table 2.** Mechanical properties of grout material.

| Grout Material | Strength(MPa) | | | Fluidity | |
|---|---|---|---|---|---|
| Time | 1 d | 3 d | 28 d | Initial | 30 min |
| M80 | 43.5 | 71.6 | 88.5 | 320 | 290 |

**Table 3.** Measured mechanical properties of rebar.

| $d_b$/mm | $f_y$/MPa | $f_u$/MPa | $\varepsilon_y/\times 10^{-6}$ | $E_s$/ MPa | ν | $A$/% |
|---|---|---|---|---|---|---|
| 18 | 375 | 620 | 2206 | 210,000 | 0.3 | 12.871 |
| 20 | 355 | 590 | 2008 | 210,000 | 0.3 | 14.807 |
| 22 | 375 | 595 | 1876 | 210,000 | 0.3 | 16.162 |
| 25 | 345 | 575 | 1604 | 210,000 | 0.3 | 16.944 |

Compared with the criterion of the Chinese core [26], the strength and fluidity of the grout meet the specification requirements.

Where $d_b$ is the diameter of rebar, $f_y$ and $f_u$ are the yield strength and the ultimate strength of rebar, respectively, $\varepsilon_y$ is the yield strain of rebar, $E_s$ is the modulus of elasticity, ν is the Poisson's ratio, and $A$ is the elongation ratio, which is the elongation of the length as a percentage of the original length.

The tensile tests of the GSS connectors were carried out with a 600 kN capacity electro-hydraulic servo universal testing machine. Figure 5 shows the test setup. Two linear variable differential transducers (LDVT) were arranged at both side of the grout sleeve to monitor the vertical deformation. Strain gauge 1 and 2 were set in the bar outside the pipe sleeve to measure the bar strain. Strain gauge 3 was set on the pipe wall along the longitudinal direction to measure the strain distribution of the sleeve during tensile loading. Strain gauge 2 was set on the pipe wall along the transverse direction to measure the hoop strain. The loading process was divided into two stages. The first stage adopted force loading until the spliced rebar yielded, and the loading rate was 0.5 MPa/s. The second stage adopted displacement control loading. The separation rate of the two chucks was no more than 20–35 mm/min.

In order to observe the strain change of the rebars and sleeves under tensile load, the strain data of the most critical cross section of the rebars and the sleeves were collected. The strain gauge placement and the measuring point arrangement on rebars and sleeve surface are shown in Figure 5.

### 2.3. Results and Analysis

#### 2.3.1. Failure Modes of GSS

The tensile test results and failure modes for GSS connectors are listed in Table 4 and shown in Figure 6, respectively. In the table, $P_{u,avg}$ is the tensile load-bearing capacity, $s_1$ is the standard derivation of tensile load-bearing capacity, $\delta_u$ is the failure displacement, $s_2$ is the standard derivation of displacement, I is the rebar rupture failure mode, while II is the bond-slip failure mode of rebar-grout.

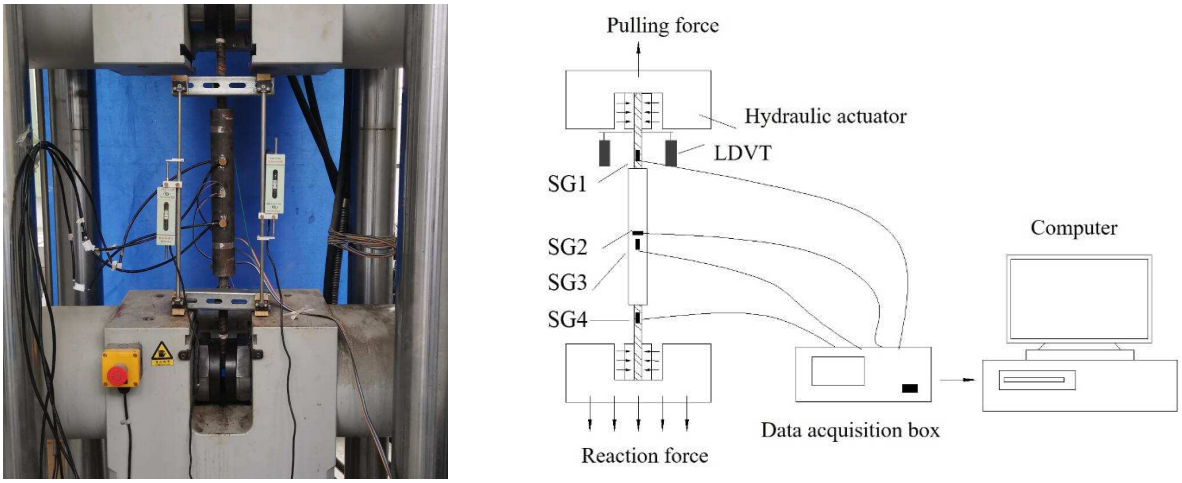


(**a**) (**b**)

**Figure 5.** Test setup. (**a**) Loading device. (**b**) Measurement program.

**Table 4.** Tensile results and failure modes.

| Types | $P_{u,avg}$/kN | $s_1$/mm | $\delta_u$/mm | $s_2$/mm | Failure Modes |
|---|---|---|---|---|---|
| D18-100% | 143.69 | 3.55 | 72.182 | 0.786 | I |
| D18-90% | 132.88 | 0.65 | 70.520 | 0.869 | I |
| D18-70% | 102.2 | 3.70 | 15.832 | 0.241 | II |
| D18-50% | 79.33 | 2.52 | 13.559 | 0.379 | II |
| D20-100% | 179.79 | 0.67 | 70.588 | 0.442 | I |
| D22-100% | 226.40 | 5.24 | 69.326 | 0.336 | I |
| D25-100% | 288.24 | 0.20 | 76.528 | 0.772 | I |

(**a**) (**b**)

**Figure 6.** Typical failure modes of the GSS connectors. (**a**) Rebar rupture failure. (**b**) Bond-slip failure of rebar-grout.

There are two failure modes for GSS connectors, namely the rebar rupture (shown in Figure 6a) and the bond-slip failure of rebar-grout (shown in Figure 6b). Figure 7 shows the load-displacement curves for all four types of fully compact GSS connectors. It can be seen that (1) the load-bearing capacity increases with the rise in the nominal diameter of sleeve and (2) the load-displacement curves are very similar to those of the rebar rupture mode. More specifically, the GSS connector shows elasticity at the initial loading stage in the load-displacement curves. As the loads increase, the grout materials crack. Following the cracks' expansion, the grout materials begin to split, internal cracks develop, and the stiffness gradually decreases, as shown in Figure 8. Obvious rebar elongation and necking deformation are observed after the yielding of rebars. The rebars rupture when the loads

reach the tensile bearing capacity. These indicate that the curves of fully compact GSS connectors are similar to the rebar constitutive relationship curves.

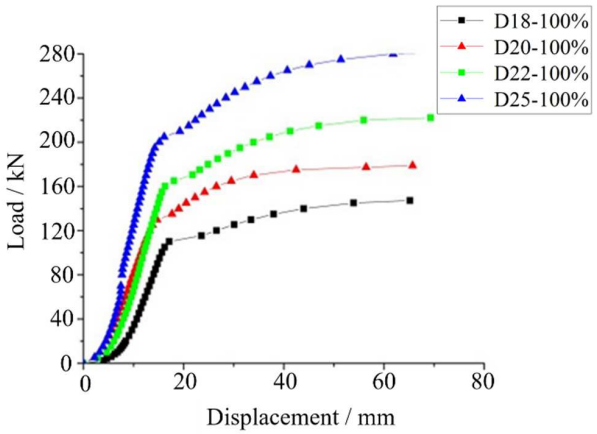


**Figure 7.** Load-displacement curves for fully compact GSS connectors.

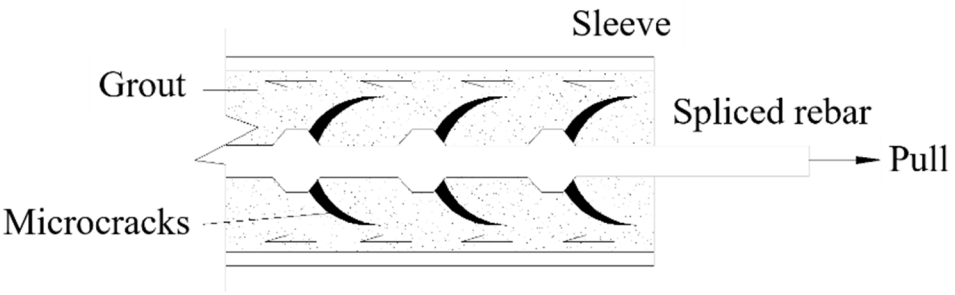


**Figure 8.** Crack expansion of grout.

Figure 9 shows the curves of D18 GSS connector at different compactness. It is shown that as the compactness decreases, the connector tensile load-bearing capacity gradually decreases as well. It can be observed at the site that the failure mode changes from the rebar rupture failure mode to the bond-slip failure mode of rebar-grout. Note that the failure mode is the bond-slip failure of rebar-grout for the GSS connector with lower compactness (D18-70% and D18-50%). It can be seen in Figure 9, for connectors with bond-slip failure of rebar-grout (D18-70% and D18-50%), that the load-displacement curves of the connectors are very similar to those of the connectors with rebar rupture failure mode before rebars yield. The load-displacement curve indicated that the specimens of D18-70% and D18-50% had no reinforcing stage and showed a rapid decline in bearing capacity. The main reason is the bond strength of rebar-grout is now less than the tensile strength of rebar, as a result of which, rebars are being pulled out.

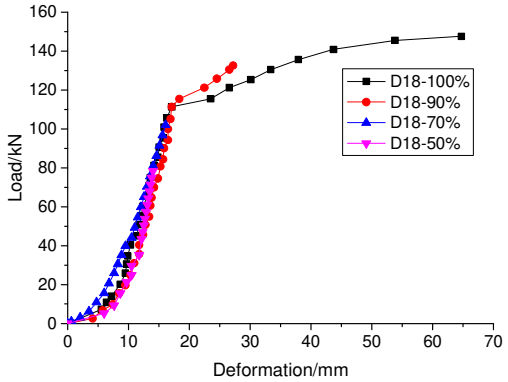


**Figure 9.** Load-displacement curves for D18 GSS connectors at different compactness.

2.3.2. Stress and Strain of Rebar

The strain of the rebar can be obtained by the stain gauge 1 and 4. The force $P$ applied to the rebar can be measured by the 600 kN capacity electro-hydraulic servo universal testing machine. Thus, the stress of the rebar can be calculated as:

$$\sigma = \frac{4P}{\pi d^2} \tag{1}$$

The rebar stress-strain curves for fully compact cases are shown in Figure 10. It can be seen that the stress-strain curves of the rebar present a linear growth trend. The curves appear jagged at both the initial stage and the ultimate tensile capacity stage. This phenomenon is caused by the fixture-reinforcement slip at the initial loading stage, the breakage of rebar-grout teeth at the final stage. The curves suddenly decline after reaching the peaks. However, the decline stage is not detected due to the limitation of test equipment or instruments. In accordance with mechanical properties of rebar (as shown in Table 4), the stresses of rebars are beyond the tensile yield stresses and amount to the tensile ultimate strengths for all four cases. This indicates that the rebars have yielded, and finally, the rebars rupture when the loads amount to the tensile ultimate load-bearing capacity.

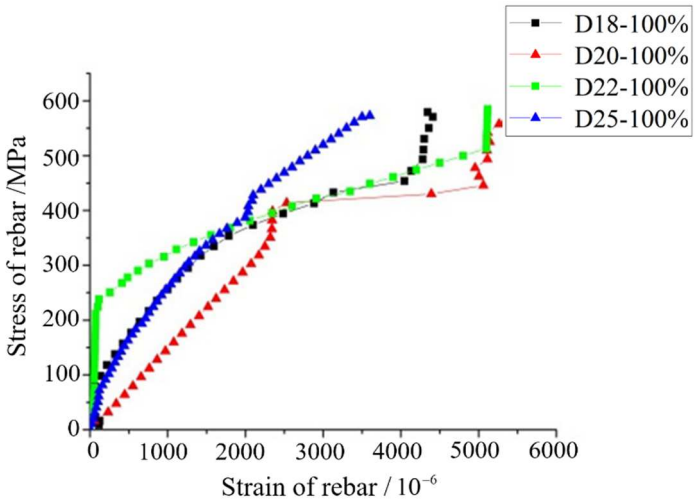


**Figure 10.** Rebar stress-strain curves for fully compact connectors.

Figure 11 shows D18 rebar stress-strain curves with different compactness. It was found that rebars of GSS connectors (D18-70%, D18-50%) have lower tensile stresses and tensile strains than those of other cases. More specifically, the maximal tensile stresses and tensile strains are all less than the yield strength and yield strain of rebar (shown in Table 4, namely 375 MPa and $2.206 \times 10^{-3}$, respectively, for GSS connects with grout compactness of 70% and 50%. The reason for this is that the connectors with lower grout compactness experience the bond-slip failure modes of rebar-grout, while other cases experience the rebar rupture failure modes (shown in Table 4). Since the bond strength of rebar-grout is less than the tensile strength of rebar, the rebars are being slowly pulled out from the GSS connectors and the connectors fail, while the stresses and strains of rebars have not fully developed and changed. Consequently, the tensile stress and strain of spliced rebars for GSS connectors with lower compactness are much lower than those of connectors with higher compactness.

The bond-slip failure mode includes the grout-pipe bond slip failure and the bar-grout bond slip failure. When the stress of the rebar is small than the strength of the bar-grout bond slip, the failure mode can be considered as the grout-pipe bond slip failure. Otherwise, it is the bar-grout bond slip failure. To clarify the failure mode of slip without breaking the sleeve, the bond strength was calculated and compared with the stress of rebar.

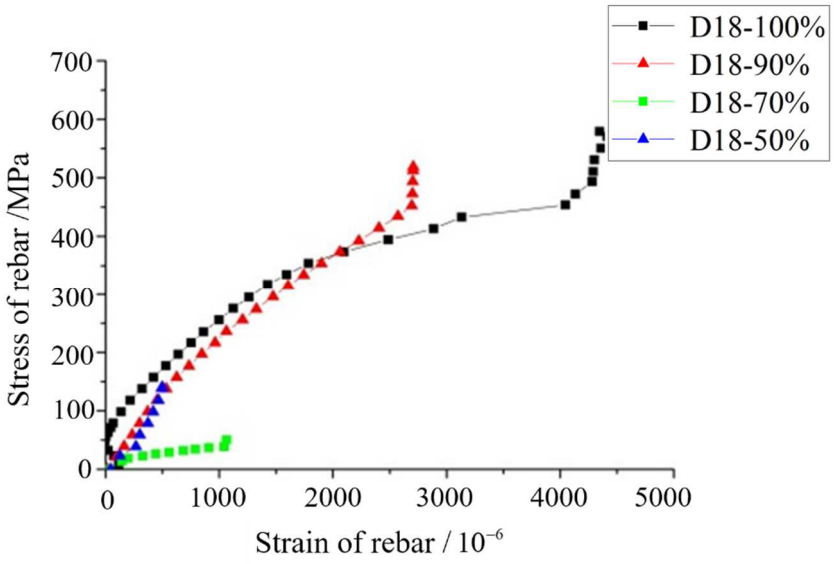


**Figure 11.** Rebar stress-strain curves for D18 connectors with different compactness.

The theoretical strength of rebar-grout bond slip can be calculated as:

$$\tau_{bg} = \frac{P_{u,\,avg}}{\pi d C L} \tag{2}$$

where $P_{u,\,avg}$ is the tensile load-bearing capacity, $d$ is the nominal diameter of rebar, $L$ is the embedded length of the rebar, and $C$ is the grout compactness.

The theoretical strength of the bar-grout bond slip was calculated and obtained in Table 5.

**Table 5.** Theoretical strength of the rebar-grout bond slip.

| Types | $P_{u,avg}$/kN | $L$/mm | $\tau_{bg}$/MPa | Failure Mode |
|---|---|---|---|---|
| D18-70% | 102.2 | 348 | 29.7 | Bond-slip |
| D18-50% | 79.33 | 348 | 32.3 | Bond-slip |

To verify the bond-slip failure mode of GSS connectors (D18-70%, D18-50%), the relevant maximum reinforcement strains were compared with the strength of the bar-grout bond slip. The results showed that the stress of the two rebars were 149.2 MPa and 52.3 MPa, respectively, and were larger than the strength of the bar-grout bond slip. This indicates that the failure mode of GSS connectors (D18-70%, D18-50%) were the bar-grout bond slip.

2.3.3. Surface Stress and Strain of Sleeve

(1) Longitudinal stress and strain

The longitudinal strain of the rebar can be obtained by the stain gauge 3. The two rebars at the upper and lower ends of the sleeve transmit force through the sleeve. Thus, the force applied to the sleeve is equal to the force $P$ applied to the rebar. Hence, the stress of the rebar can be calculated as:

$$\sigma = \frac{4P}{\pi(D - d_{si})^2} \tag{3}$$

The longitudinal stress-strain curves for all four cases with full compactness are shown in Figure 12. It can be seen that the longitudinal stress-strain curves show a linear growth trend. As the tensile capacity of the sleeve is approached, the curves do not present plateau like those for the rebars. The maximal values of the longitudinal tensile stresses are less

than 300 MPa for all four kinds of sleeves. The rated tensile strength of the sleeves is 550 MPa according to the manufacturer, which means the stress of the sleeve is still within its tensile strength. As can be seen, there is still a great surplus of longitudinal tensile stress. However, the decline stage is not recorded due to the limitation of test equipment and instruments. After a comparison is made with the longitudinal stress of the sleeve (Figure 12) and the stress of rebars (as seen in Figure 10 and Table 4), it was found that the maximal stress cross-sections are not within the length of the sleeves but within the length of outer rebars for all four kinds of sleeves. The reason for this is that the sleeve, grout, and spliced rebars together bear the tensile load at the GSS section, while the outer rebars uniquely bear the tensile load. Therefore, the failure modes are rebar rupture for all four kinds of sleeves.

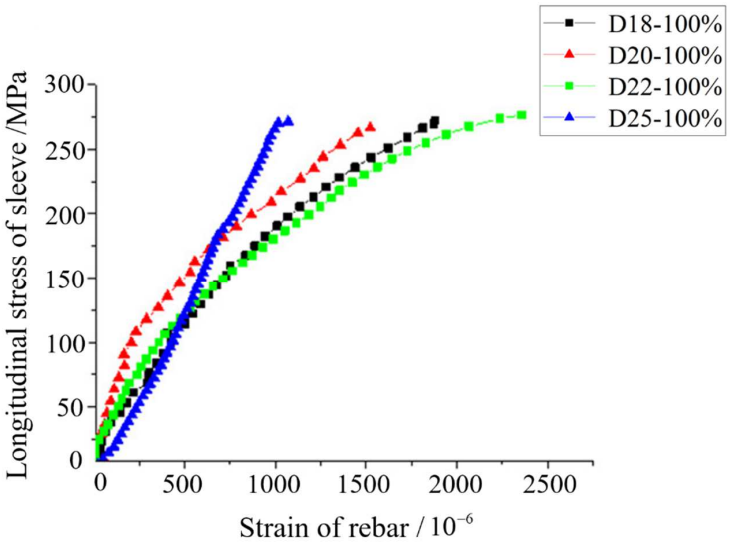


**Figure 12.** Longitudinal stress-strain curves of sleeve for fully compact connectors.

The stress-strain curves of sleeves for D18 connectors with different compactness are shown in Figure 13. The observed phenomenon and laws are similar to those of rebar for the connectors with different compactness (as shown in Figure 11). The sleeves of GSS connectors have much lower tensile stresses and tensile strains. The maximal tensile stresses and tensile strains are less than 100 MPa for sleeves with lower compactness (D18-70%, D18-50%), which means the sleeves are still in the elastic stage. The curves drop abruptly in their rise due to either the snap of the rebar or the bond-slip of the rebar-grout. It is noteworthy that the longitudinal stress-strain curves of D18-90% sleeves in Figure 13 show abnormality. One possible reason for this is that a closure of cracks in the grouting material has occurred at loading and it has a greater effect than the newly developed cracks in the grouting material.

(2) Load and hoop strain $\varepsilon_{t,sl}$

The splitting deformation of grouting material is very small at the early loading stage. In this stage, the Poisson's effect dominates, and the hoop strain of the sleeve is compressive strain. As the splitting deformation of grouting material increases to a certain extent, the hoop strain gradually develops to tensile strain [9]. Figure 14 shows the load-hoop strain curves of all four fully compact cases. Figure 15 shows load-hoop strain curves of the sleeve for the D18 connector with different compactness. It can be seen that the sleeve hoop strain is compressive strain, the grouting material splitting deformation is small, and the hoop strain never goes into tensile strain. In addition, the hoop strains and loads are all very low, namely lower to $1.10 \times 10^{-4}$ and 42 kN, respectively, for sleeves with lower compactness (D18-70%, D18-50%). This is because their failure modes are the bond-slip failure modes of rebar-grout. Through the above analysis, the hoop strain $\varepsilon_{t,sl}$ can be used as the basis for calculating the transverse tensile stress of the sleeve in Section 3.

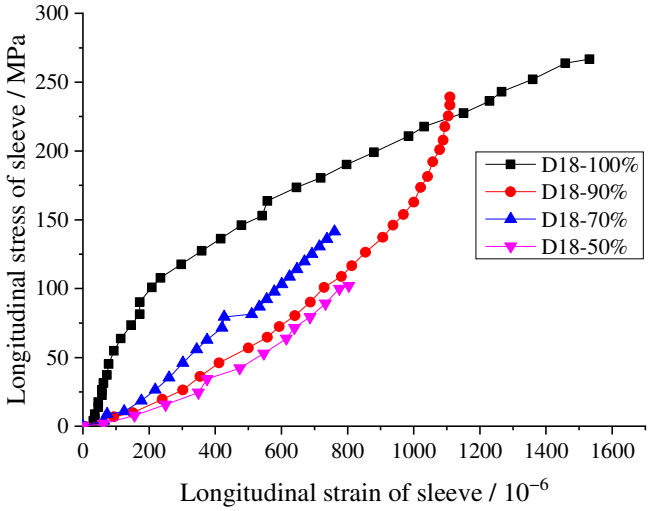


**Figure 13.** Longitudinal stress-strain curves of sleeve for D18 connectors with different compactness.

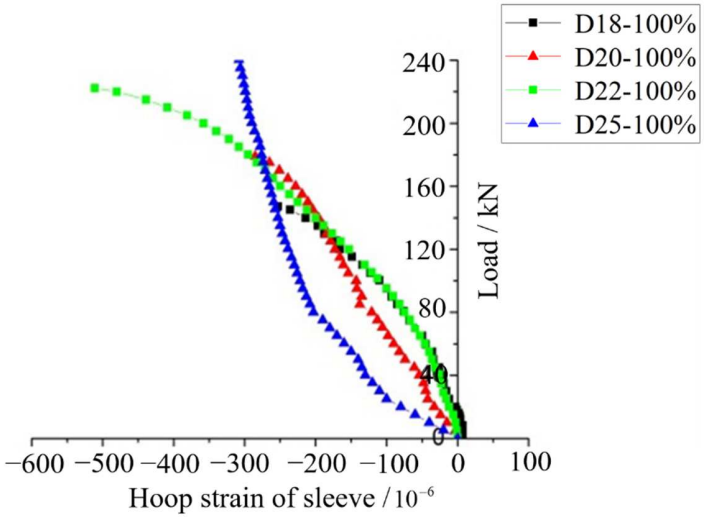


**Figure 14.** Load-hoop strain curves of sleeves for fully compact connectors.

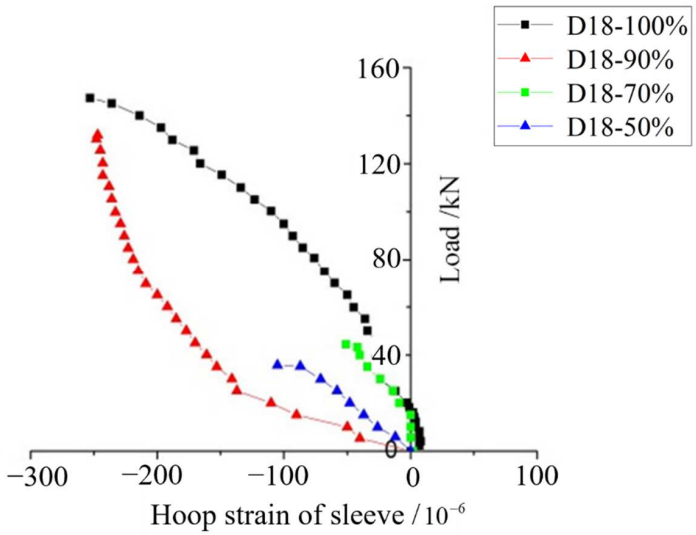


**Figure 15.** Load-hoop strain curves of the sleeve for the D18 connector with different compactness.

## 3. Tensile Bearing Capacity of Grouted Splice Sleeve

There is a great difference in the processing technology and structural construction of grouted splice sleeves both at home and abroad, different performance, and different calculation theories were developed for different types of GSS [1,3,4,7–9,18,19].

In light of a lacking existing bond-slip model of rebar-grout in spliced sleeve, this section first analyzes the load transfer mechanism of GSS and then deduces the bond-slip model of the rebar-grout. Lastly, the formula is proposed for calculating the tensile bearing capacity of GSS.

### *3.1. The Bond-Slip Model for Rebar-Grout*

Based on the aforementioned tests and related references [3–9,18,19], the force transfer path of grouted splice sleeve is ascertained as follows: force→one side of rebar→grouting material→sleeve→grout→the other side of rebar. The constraint effect of the sleeve restricts the splitting of the grouting material, significantly improves the bonding strength of the rebar-grout, and greatly shortens the anchorage length of the spliced rebar.

In order to derive the bond-slip model of rebar-grout material, the following assumptions are made:

(1) The constraint stress $u_n$ of the sleeve acting on the grout material is evenly distributed;
(2) The constraint stress $u_n$ can be calculated and quantified by the transverse strain of sleeve, $\varepsilon_{t,sl}$;
(3) The bonding stress of rebar-grout $u_b$ is uniformly distributed in the range of the anchorage length of rebar;
(4) The bonding force of the sleeve acting on the grout equals the bonding force of the grout acting on the rebar;
(5) Derivation is based on a fully compact connector; the derived formula is used in the compact and incompact connectors. Moreover, an incompact connector is considered as a compact connector with a lower bearing capacity.

Figure 16 shows the relationship between the transversely tensile force of spliced sleeve $T_{t,sl}$ and the constraint stress of sleeve acting on grout material $u_n$.

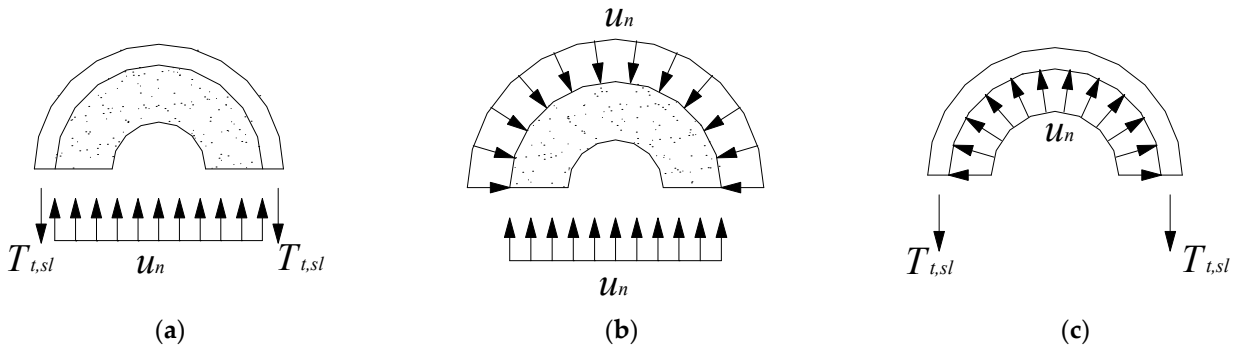


**Figure 16.** Stress diagram of the isolated body for the grouted splice sleeve. (**a**) Sleeve-grout. (**b**) Grout. (**c**) Sleeve.

The transverse tensile stress of sleeve $f_{t,sl}$ is a function of sleeve strain $\varepsilon_{t,sl}$ and sleeve elastic modulus $E_{sl}$, and the sleeve strain $\varepsilon_{t,sl}$ can be obtained from Figures 14 and 15. $f_{t,sl}$ is expressed as:

$$f_{t,sl} = \varepsilon_{t,sl} E_{sl} \tag{4}$$

where $f_{t,sl}$ is controlled by the longitudinal section area of sleeve.

The grout incompactness will decrease the bonding area between the grout and the sleeve. This will reduce the bearing capacity, and then decreasing the transversely tensile force of spliced sleeve $T_{t,sl}$. When the incompact connector is considered as a compact connector with a lower bearing capacity based on the fifth assumption, the value of $T_{t,sl}$ will

be overestimated if the reduction of the bonding area is ignored. Because the bonding force of sleeve acting on grout material is equal to the bonding force of grout material acting on rebar. Thus, the reduction of the bonding area can be translated to the decrease of the anchorage length of the rebar. $T_{t,sl}$ is expressed as:

$$f_{t,sl} = \frac{T_{t,sl}}{t_{sl} l_c} \tag{5}$$

$$l_c = C l_b \tag{6}$$

where $t_{sl}$ is the sleeve wall thickness, $l_b$ is the anchorage length of rebar, and $C$ is the incompactness coefficient; its value can be taken as 1.0, 0.9, and 0.7 when the grout compactness is 100%, 90%, 70%, respectively.

$$T_{t,sl} = \varepsilon_{t,sl} C l_b t_{sl} E_{sl} \tag{7}$$

According to the static equilibrium, we have the following equation (shown in Figure 16a):

$$2T_{t,sl} = u_n d_{si} l_b \tag{8}$$

where $d_{sl}$ is the internal diameter of the sleeve.

Substitute Equation (7) into Equation (8), and the constraint stress $u_n$ is obtained as:

$$u_n = \frac{2C\varepsilon_{t,sl} t_{sl} E_{sl}}{d_{si}} \tag{9}$$

The bonding force of sleeve acting on grout material $F_n$ is the product of the confining stress of sleeve acting on grout material $u_n$ and the inner surface area of sleeve $A_{c,sl}$:

$$F_n = u_n A_{c,sl} \tag{10}$$

where $A_{c,sl} = \pi d_{si} l_b$.

Because the bonding force of sleeve acting on grout material is equal to the bonding force of grout material acting on rebar, the restraint stress of grout material acting on rebar $u_{n,\,b}$ is obtained as:

$$u_{n,b} = \frac{\pi d_{si} l_b u_n}{\pi d_b l_b} = \frac{d_{si} u_n}{d_b} \tag{11}$$

where $d_b$ is the diameter of the spliced rebar.

The increase of the bonding stress of rebar-grout material $u_b$ is proportional to the square root of the bonding force of grout material acting on rebar $u_{n,b}$ and the compressive strength of the grout material $f_{u,g}$ [30], then:

$$u_b = (A + B\sqrt{u_{n,b}})\sqrt{f_{u,g}} \tag{12}$$

where $A$ and $B$ are the constant term and the coefficient of the linear expression obtained by fitting with the test results. According to the experimental results, $A$ and $B$ are fitted to be 0.3612 and 0.2101, respectively (Figure 17).

The bonding force of rebar-grout material $P_b$, is calculated by multiplying the bonding stress $u_b$, and the contact area of rebar-grout material:

$$P_b = \pi d_b l_b u_b \tag{13}$$

Substitute Equation (12) into Equation (13), then:

$$P_b = \pi d_b l_b (A + B\sqrt{u_{n,b}})\sqrt{f_{u,g}} \tag{14}$$

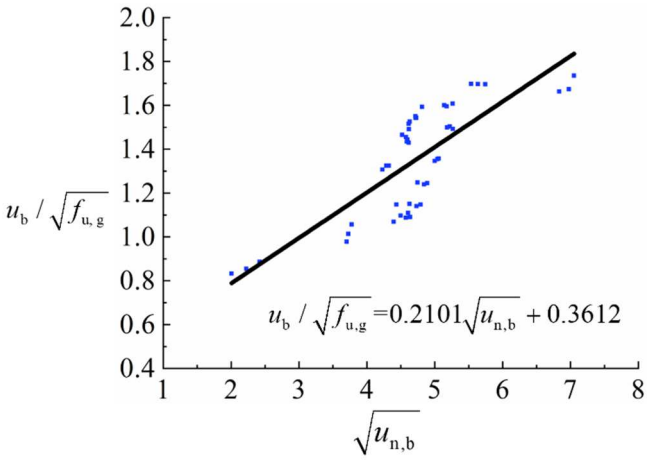


**Figure 17.** Fitting curve of $u_b/\sqrt{f_{u,g}}$ and $\sqrt{u_{n,b}}$.

It is known from the experimental results and formula derivation process that the size of the sleeve will affect the restraint stress of grout material acting on rebar, $u_{n,b}$. Substitute $A$ = 0.3612, $B$ = 0.2101 and Equation (11) into Equation (14), then:

$$P_b = \pi l_b \sqrt{d_b f_{u,g}}(0.3612\sqrt{d_b} + 0.2101\sqrt{d_{si}u_n}) \tag{15}$$

Substituting Equation (8) into the second term of Equation (12), we obtain:

$$0.2101\sqrt{d_{si}u_n} = (0.2101 \times \sqrt{2}) \times \sqrt{C\varepsilon_{t,sl}t_{sl}E_{sl}} = 0.297\sqrt{C\varepsilon_{t,sl}t_{sl}E_{sl}} \tag{16}$$

As a result, the bonding force rebar-grout material $P_b$ can be obtained by Equation (15). The derivation process of $P_b$ indicates that the calculation of the bond strength of rebar-grout material must take into consideration the following parameters, namely the bar diameter $d_b$, the anchorage length of spliced rebar $l_b$, and material properties $f_{u,g}$, $E_{sl}$, and $\varepsilon_{t,sl}$.

### *3.2. Tensile Bearing Capacity of Grouted Splice Sleeve*

The tensile bearing capacity of spliced rebar, $T_b$, is given as [4]:

$$T_b = k_2 \pi f_y (\frac{d_b^2}{4}) \tag{17}$$

where $k_2$ is the average value of the ratio of tensile strength and yield strength of rebar, which is 1.642 according to Table 4 [4].

In accordance with Equations (15) and (17), the tensile capacity of grouted splice sleeve, $P_u$, is determined by the smaller one of $P_b$ and $T_b$, thus:

$$P_u = \begin{cases} P_b, P_b \le T_b \\ T_b, \text{else} \end{cases} \tag{18}$$

### *3.3. Experimental Verification*

In order to verify the effectiveness and reliability of the formulas derived for calculating the tensile capacity of GSS, the above experimental results are substituted into the derived formulas, and the results are shown in Table 6. Notation I stands for the rebar rupture failure mode and II is the bond-slip failure mode of rebar-grout. $P_{u,e}$ and $P_{u,c}$ are the experimental tensile bearing capacity and the calculated value, respectively, $\sigma_r$ is the standard derivation of $P_{u,c}$, $R_r$ is the ratio between the experimental values $P_{u,e}$ and calculated values $P_{u,c}$ for the GSS tensile capacity, and the reduced value of the tensile capacity calculation in the case of incompact grouting is represented with $P_{u,c}{}^0$.

$$R_r = \frac{P_{u,e}}{P_{u,c}} \tag{19}$$

$$P_{u,c}^0 = \left| \frac{P_{u,c\ (90\%\ \text{or}\ 70\%\ \text{or}\ 50\%)} - P_{u,c\ (100\%)}}{P_{u,c(100\%)}} \right| \tag{20}$$

**Table 6.** Prediction results.

| Types | $T_b$/kN | $P_b$/kN | $P_{u,c}$/kN | $P_{u,c}{}^0$/% | $P_{u,e}$/kN | Mode | $R_r$ | $\sigma_r$ |
|---|---|---|---|---|---|---|---|---|
| D18-100% | 156.69 | 125.14 | 125.14 | 0 | 143.69 | II | 1.15 | 1.89 |
| D18-90% | 156.69 | 122.92 | 122.92 | 1.8 | 132.88 | II | 1.08 | 0.30 |
| D18-70% | 156.69 | 119.84 | 119.84 | 4.2 | 102.20 | II | 0.85 | 1.01 |
| D18-50% | 156.69 | 76.55 | 76.55 | 38.8 | 79.33 | II | 1.04 | 4.02 |
| D20-100% | 183.13 | 163.09 | 163.09 | 0 | 179.79 | II | 1.10 | 1.51 |
| D22-100% | 234.07 | 244.11 | 234.07 | 0 | 226.40 | I | 0.97 | 3.10 |
| D25-100% | 278.08 | 262.70 | 262.70 | 0 | 288.24 | II | 1.10 | 3.72 |

Due to the non-uniform material quality and the assumptions made in the derivation process, the data for $u_b$ appear discretized, when $\sqrt{u_{n,b}}$ is in the range of 4.00~6.00 (Figure 6). It can be seen that the experimental results $P_{u,e}$ are comparatively in agreement with the calculated value of tensile capacity $P_{u,c}$. The value of the ratio between the experimental values $P_{u,e}$ and calculated values $P_{u,c}$, $R_r$, fluctuates in the range of 0.85 to 1.15. The maximum value of the standard deviation of the calculated tensile capacity $\sigma_r$ is 3.72, and the predicted results are still acceptable.

## 4. Conclusions and Remarks

(1) The grout compactness determines the failure modes of GSS connectors. Generally, the failure mode of GSS connectors with higher grout compactness is rebar rupture, while the failure mode of GSS connectors with lower compactness is the bond-slip failure mode of rebar-grout.
(2) The tensile tests of GSS with different compactness showed that the tensile bearing capacity decreases with the decrease of grout compactness. For example, when the compactness is 50%, the tensile capacity of the sleeve is close to 60% of the fully compact tensile capacity.
(3) The bond-slip model of rebar-grout material is deduced and the formula of tensile bearing capacity of GSS with the grout compactness into consideration is proposed in this paper. The proposed formula can be used to determine whether reinforcing remedies or re-grouting is needed for sleeves that are not fully grouted during construction.

All in all, the grout compactness has become the dominant factor for failure modes and bearing capacity of GSS connectors, and the proposed tensile bearing capacity formula of GSS can be used to determine whether reinforcing remedies or re-grouting is required in the case of incompact sleeve grouting during construction. Note that the above-mentioned conclusions and remarks are only validated by limited experimental results, and more experimental data and numerical simulation are needed to validate the proposed models and methods in the future.

**Author Contributions:** S.J., Z.Z. and W.C. designed the experiment; Z.Z., W.C. and C.Z. performed the experiments and wrote the paper; S.J. revised and finalized the paper. All authors have read and agreed to the published version of the manuscript.

**Funding:** The work was supported by the National Key R&D Program of China (Grant No. 2016YFC0700700) and the Key R&D Program of Fujian Science & Technology Department (Grant No. 2017Y4012). In addition, the authors are appreciated to the anonymous referees for their constructive comments and valuable suggestions.

**Institutional Review Board Statement:** Not applicable.

**Informed Consent Statement:** Not applicable.

**Data Availability Statement:** Not applicable.

**Conflicts of Interest:** The authors declare no conflict of interest.

## References

1. Chinese Academy of Architectural Sciences. *Grouting Sleeve for Reinforcement Connection*; JG/T398-2012; China Architecture & Building Press: Beijing, China, 29 October 2012.
2. Chinese Academy of Architectural Sciences. *Cementitious Grout for Rebar Sleeve Slicing*; JG/T408-2013; China Architecture & Building Press: Beijing, China, 24 May 2013.
3. Ling, J.H.; Abd Rahman, A.B.; Ibrahim, I.S.; Hamid, Z.A. Behaviour of grouted pipe splice under incremental tensile load. *Constr. Build. Mater.* **2012**, *33*, 90–98. [CrossRef]
4. Ling, J.H.; Abd Rahman, A.B.; Ibrahim, I.S.; Hamid, Z.A. Tensile capacity of grouted splice sleeves. *Eng. Struct.* **2016**, *111*, 285–296. [CrossRef]
5. Wu, X.B.; Lin, F.; Wang, T. Experimental study on effect of age and rebar type on mechanical performance of reinforced cylinder grouting connections. *Build. Struct.* **2013**, *14*, 77–82.
6. Zheng, Y.; Guo, Z.; Cao, J. Confinement mechanism and confining stress distribution of new grouting coupler for rebars splicing. *J. Harbin Inst. Technol.* **2015**, *47*, 106–111.
7. Wang, D.H.; Liu, X.D.; Liu, Y.L. Experimental study on tensile ultimate capacity of cement grouting connectors. *Build. Struct.* **2015**, *6*, 21–23.
8. Zheng, Y.; Guo, Z. Experimental study and finite element analysis on behavior of deformed gout-filled pipe splice. *J. Build. Struct.* **2016**, *37*, 94–102.
9. Chen, X.N. Research on Connection Technology of New Grouting Steel Sleeve. Master's Thesis, Southeast University, Nanjing, China, 2015.
10. Tullini, N.; Minghini, F. Grouted sleeve connections used in precast reinforced concrete construction—Experimental investigation of a column-to-column joint. *Eng. Struct.* **2016**, *127*, 784–803. [CrossRef]
11. Xu, G.S.; Wang, Z.; Wu, B.; Bursi, O.S.; Tan, X.J.; Yang, Q.B.; Wen, L. Seismic performance of precast shear wall with sleeves connection based on experimental and numerical studies. *Eng. Struct.* **2017**, *150*, 346–358. [CrossRef]
12. Popa, V.; Papurcu, A.; Cotofana, D.; Pascu, R. Experimental testing on emulative connections for precast columns using grouted corrugated steel sleeves. *Bull. Earthq. Eng.* **2015**, *13*, 2429–2447. [CrossRef]
13. Ameli, M.J.; Pantelides, C.P. Seismic Analysis of Precast Concrete Bridge Columns Connected with Grouted Splice Sleeve Connectors. *J. Struct. Eng.* **2017**, *143*, 4016176. [CrossRef]
14. Li, J.; Hao, H.; Xia, Y.; Zhu, H.P. Damage assessment of shear connectors with vibration measurements and power spectral density transmissibility. *Struct. Eng. Mech.* **2015**, *54*, 257–289. [CrossRef]
15. Li, J.; Hao, H. Health monitoring of joint conditions in steel truss bridges with relative displacement sensors. *Measurement* **2016**, *88*, 360–371. [CrossRef]
16. Jiang, T.Y.; Kong, Q.Z.; Wang, W.X.; Huo, L.S.; Song, G.B. Monitoring of Grouting Compactness in a Post-Tensioning Tendon Duct Using Piezoceramic Transducers. *Sensors* **2016**, *16*, 1343. [CrossRef] [PubMed]
17. Liu, H.; Li, X.M.; Xu, Q.F. Test on detection of grouting compactness of grout sleeve by impact-echo method. *Nondestruct. Test* **2017**, *39*, 12–16.
18. Yuan, H.; Zhu, Z.G.; Naito, C.J.; Yi, W.J. Tensile behavior of half grouted sleeve connections: Experimental study and analytical modeling. *Constr. Build. Mater.* **2017**, *152*, 96–104. [CrossRef]
19. Zheng, Y.F.; Guo, Z.X.; Liu, J.B.; Chen, X.N.; Xiao, Q.D. Performance and confining mechanism of grouted deformed pipe splice under tensile load. *Adv. Struct. Eng.* **2016**, *19*, 86–103. [CrossRef]
20. Parks, J.E. Seismic Rehabilitation of Column to Pier Cap Accelerated Bridge Construction Connections and Acoustic Emission Monitoring Assessment. Ph.D. Thesis, The University of Utah, Salt Lake City, UT, USA, 2014.
21. Parks, J.E.; Papulak, T.; Pantelides, C.P. Acoustic emission monitoring of grouted splice sleeve connectors and reinforced precast concrete bridge assemblies. *Constr. Build. Mater.* **2016**, *122*, 537–547. [CrossRef]

22. Chen, J.W.; Wang, Z.W.; Liu, Z.Y.; Ju, S.L. Experimental investigation of mechanical properties of steel half-grouted sleeve splice with rebar bonding defects. *J. Build. Eng.* **2022**, *50*, 104113. [CrossRef]
23. Lu, Z.W.; Wu, B.; Yang, S.P.; Hou, J.Y.; Ji, Z.Z.; Li, Y.F.; Huang, J.; Zhang, M.Z. Experimental study on flexural behaviour of prefabricated concrete beams with double-grouted sleeves. *Eng. Struct.* **2021**, *248*, 113237. [CrossRef]
24. Yu, Q.; Zhang, L.; Bai, S.H.; Fan, B.X.; Chen, Z.H.; Li, L.Z. Experimental Study on Seismic Behavior of Precast Frame Columns with Vertical Reinforcement Spliced with Grouted Sleeve Lapping Connectors. *Adv. Civ. Eng.* **2021**, *2021*, 1549303. [CrossRef]
25. Xiao, S.; Wang, Z.L.; Li, X.M.; Harries, K.A.; Xu, Q.F.; Gao, R.D. Study of effects of sleeve grouting defects on the seismic performance of precast concrete shear walls. *Eng. Struct.* **2021**, *236*, 111833. [CrossRef]
26. Chinese Academy of Architectural Sciences. *Technical Specification for Grout Sleeve Splicing of Rebars*; JGJ355-2015; China Architecture & Building Press: Beijing, China, 9 January 2015.
27. Chinese Academy of Building Materials Science. *Strength Testing Method for Cement Mortar*; GB/T17671-1999; China Architecture & Building Press: Beijing, China, 2 February 1999.
28. China Vanke. *Technical Specification for Prefabricated Integral Reinforced Concrete Structure*; SJG18-2009; China Architecture & Building Press: Beijing, China, 30 September 2009.
29. Chinese Iron and Steel Research Institute. *Tensile Testing of Metallic Materials-Part 1: Test Methods for Temperature*; GB/T1228.1-2010; China Quality Inspection Press: Beijing, China, 23 December 2010.
30. Untrauer, R.E.; Henry, R.L. Influence of normal pressure on bond strength. *J. Proc.* **1965**, *62*, 577–585.